Probing the electronic properties of dichromium oxide clusters $Cr_2O_n^-$ (n=1–7) using photoelectron spectroscopy

Hua-Jin Zhai and Lai-Sheng Wang[a)]
Department of Physics, Washington State University, Richland, Washington 99354
and Chemical Sciences Division, Pacific Northwest National Laboratory, Richland, Washington 99352

(Received 5 September 2006; accepted 13 September 2006; published online 25 October 2006)

In an effort to elucidate the variation of the electronic structure as a function of oxidation and composition, we investigated an extensive series of dichromium oxide clusters, $Cr_2O_n^-$ (n=1–7), using photoelectron spectroscopy (PES). Well-resolved PES spectra were obtained at several photon energies. While low photon energy spectra yielded much better spectral resolution, high photon energy data allowed both Cr 3*d*- and O 2*p*-derived detachment features to be observed. The overall spectral evolution of $Cr_2O_n^-$ exhibits a behavior of sequential oxidation with increasing oxygen content, where low binding energy Cr 3*d*-based spectral features diminish in numbers and the spectra shift towards higher binding energies as a result of charge transfer from Cr to O. Evidence was obtained for the population of low-lying isomers for $Cr_2O_2^-$, $Cr_2O_3^-$, and $Cr_2O_6^-$. The current data are compared with previous studies and with related studies on $W_2O_n^-$ and $Mo_2O_n^-$. © *2006 American Institute of Physics*. [DOI: 10.1063/1.2360531]

I. INTRODUCTION

Chromium oxides are important materials with broad technological applications.[1] Chromium oxide-based catalysts are responsible for numerous industrial processes,[2] whereas CrO_2 is widely used in magnetic recording tapes and other thin film applications.[3,4] Both the catalytic activity and magnetic properties of chromium oxides are closely dependent on their compositions. In the gas phase, dichromium oxide clusters[5–16] and bare Cr_2 dimer[17–24] are intriguing species. Chromium possesses a unique half-filled $3d^54s^1$ electronic configuration. In Cr_2, antiferromagnetic spin coupling leads to a $^1\Sigma_g^+$ singlet ground state and a formal bond order of six.[17–24] The Cr_2^- anion also has an antiferromagnetic spin coupling and a magnetic moment of $1\mu_B$.[20] However, the Cr_2^+ cation was recently predicted by density functional theory (DFT) calculations to possess a ferromagnetic spin coupling and a high magnetic moment of $11\mu_B$.[24] Reddy *et al.*[5,6] conducted DFT calculations on Cr_2O_n (n=1–6) clusters and found oscillatory magnetic coupling as a function of n. Pandey and co-workers[7,8] also reported DFT studies on Cr_2O_n (n=1–4). More recently, Kondow and co-workers[9,10] reported a combined photoelectron spectroscopy (PES) and DFT study on Cr_2O^-, $Cr_2O_2^-$, and $Cr_2O_3^-$. They found highly spin-polarized electronic structure and ferromagnetic coupling in these clusters and raised the interesting possibility of chemical control of magnetism.

We have been interested in understanding the structural and electronic properties of transition metal oxide clusters, which are used as molecular level models for the complicated catalytic surfaces and for providing possible mechanistic insight into the catalytic activity. The current work represents a continuation of our research interest in metal oxide clusters.[25–38] Among our previous PES studies is the characterization of a series of monochromium oxide clusters, CrO_n^- and CrO_n (n=1–5).[31] In another closely relevant recent work,[34,35] we have characterized the electronic and structural properties of $W_2O_n^-$ (n=1–7). We have found superoxide species[38] and *d*-orbital aromaticity[36] in tungsten oxide clusters. Jarrold and co-workers have recently investigated the electronic structure and chemical reactivity of several related dimolybdenum oxide clusters.[39,40]

Here we report a PES study of a complete series of dichromium oxide clusters $Cr_2O_n^-$ ranging from n=1 to 7 systematically at several photon energies. Significantly better resolved spectra have been obtained for n=1–3 and are compared with the previous studies.[9,10] As a result, several major reassignments are made. We have observed that the overall PES spectral evolution displays a behavior of sequential oxidation with increasing oxygen content. Evidence is also obtained for the coexistence of isomers for $Cr_2O_2^-$, $Cr_2O_3^-$, and $Cr_2O_6^-$. Electron affinities are obtained for all the neutral Cr_2O_n clusters, which are observed to increase with n due to the sequential oxidation. Comparisons with the related isoelectronic systems, $W_2O_n^-$ and $Mo_2O_n^-$, are also made.

II. EXPERIMENTAL METHOD

The experiment was carried out using a magnetic-bottle-type PES apparatus equipped with a laser vaporization supersonic cluster source, details of which have been described previously.[41,42] Briefly, chromium oxide cluster anions were produced by laser vaporization of a pure chromium target in the presence of a helium carrier gas seeded with 1% N_2O or 0.5% O_2. Various $Cr_mO_n^-$ clusters were produced from the source and analyzed using a time-of-flight mass spectrometer. The $Cr_2O_n^-$ (n=1–7) species of current interest were each mass selected and decelerated before being photodetached. Four detachment photon energies were used in the

a)Electronic mail: ls.wang@pnl.gov

present study: 532 nm (2.331 eV), 355 nm (3.496 eV), 266 nm (4.661 eV), and 193 nm (6.424 eV). Photoelectrons were collected at nearly 100% efficiency by the magnetic bottle and analyzed in a 3.5-m-long electron flight tube. The photoelectron spectra were calibrated using the known spectrum of Rh^-, and the energy resolution of the PES apparatus was $\Delta Ek/Ek \sim 2.5\%$, that is, ~25 meV for 1 eV electrons.

It was noted that the highly oxygen deficient species (e.g., Cr_2O^- and $Cr_2O_2^-$) were extremely reactive and had exhibited very low abundance when the 0.5% O_2 or 1% N_2O seeded helium carrier gas was used. Instead, they were produced with a pure helium carrier gas as impurities, where oxide contamination on the target surface or residual oxygen inside the nozzle served as the oxygen source. We also found that both 0.5% O_2 and 1% N_2O seeded helium carrier gases were good oxygen sources to produce the $Cr_2O_n^-$ clusters; but the N_2O-seeded He carrier gas represented a more gentle oxygen source and tended to produce relatively colder oxide clusters. We have shown previously that cluster temperature control is essential for high quality PES experiments.[43–46] All data presented in the current study were obtained using the He carrier gas seeded with 1% N_2O or pure He carrier gas, unless specifically stated otherwise.

III. RESULTS

The PES spectra for $Cr_2O_n^-$ ($n=1-6$) at different photon energies are shown in Figs. 1–8, whereas Fig. 9 compares all the spectra for $n=1-7$ at 193 nm. The observed electronic transitions are labeled with letters and the measured adiabatic detachment energy (ADE) and vertical detachment energy (VDE) and vibrational frequencies are summarized in Table I.

TABLE I. Observed adiabatic and vertical detachment energies and vibrational frequencies from the photoelectron spectra of $Cr_2O_n^-$ ($n=1-6$).

Species	Observed feature	ADE (eV)[a,b]	VDE (eV)[a]	Vibrational frequency (cm^{-1})[a]
Cr_2O^-	X'	0.9 (1)	~1.1	
	X		1.17 (3)	
	A		1.71 (2)	
	B		1.95 (2)	
	C		2.12 (2)	
	D		2.61 (4)	
	E		3.20 (4)	
$Cr_2O_2^-$	X	1.65 (3)	1.69 (3)	
	A		2.52 (2)	890 (50)
	B		2.99 (3)	
	C		3.16 (5)	
	D		3.81 (5)	
$Cr_2O_3^-$	X	1.68 (2)	1.83 (5)	620 (30), 280 (30)
	A		2.36 (5)	
	B		3.01 (3)	
	C		3.14 (3)	
	D		3.71 (5)	
	E		4.16 (5)	
$Cr_2O_4^-$	X	2.55 (3)	2.84 (5)	630 (50)
	A		4.12 (3)	
	B		4.70 (5)	
	C		5.62 (5)	
	D		6.28 (5)	
$Cr_2O_5^-$	X	3.49 (2)	3.82 (5)	710 (50)
	A		4.58 (5)	
	B		5.17 (3)	
	C		5.60 (5)	
	D		6.13 (3)	
$Cr_2O_6^-$	X	4.28 (2)	4.45 (5)	780 (50)
	A		5.98 (2)	
	B		6.28 (3)	

[a]The numbers in parentheses represent experimental uncertainties in the last digits.
[b]The ADE also represents the electron affinity of corresponding neutral species.

A. Cr_2O^-

The PES spectra of Cr_2O^- at four photon energies are shown in Fig. 1, which revealed complicated and congested electronic transitions. The 532 nm spectrum [Fig. 1(a)] revealed four relatively sharp bands (X, A, B, and C). However, the lowest energy band ranging from 0.7 to 1.5 eV appeared to consist of an intense and sharp feature (X) sitting on top of a broad band (X'). X and X' were likely due to two overlapping electronic transitions. The VDE of the X' band was estimated to be ~1.1 eV. Since no vibrational structures were resolved for the X' band, the ADE was estimated by drawing a straight line at its leading edge on the low energy side, and then adding the instrumental resolution to the intersection with the binding energy axis. For sharp spectral onsets, this method can yield relatively accurate and consistent ADE values. However, for Cr_2O^-, the obtained value, 0.9 ± 0.1 eV, should be viewed as the upper limit for the ADE due to the broad nature of band X', which indicates a large geometry change between the ground states of Cr_2O^- and Cr_2O. Features X, A, B, and C were all very sharp and well defined; their VDEs were measured to be 1.17, 1.71, 1.95, and 2.12 eV, respectively.

The 355 nm spectrum showed more complicated features at higher binding energies [Fig. 1(b)]. Band D was tentatively labeled, which became better defined in the 266 and 193 nm spectra. But there were likely unresolved electronic transitions in the energy ranges around bands C and D from 2.1 to 3 eV. Band E was very sharp with a VDE of 3.20 eV in the 266 nm spectrum. The high photon energy spectra at 266 and 193 nm did not produce any additional well-resolved transitions and revealed essentially continuous signals beyond 3 eV.

B. $Cr_2O_2^-$

The spectra of $Cr_2O_2^-$ at four detachment photon energies are shown in Fig. 2. One major band (X) was observed at 532 nm with a VDE of 1.69 eV and an ADE of 1.65 eV. This band exhibited discernible fine features with an average spacing <300 cm^{-1}, which was likely due to a low frequency bending mode. Very weak signals (X') were present at low binding energies around ~1.2 eV. The extremely low intensity of this band suggested that it probably came from a

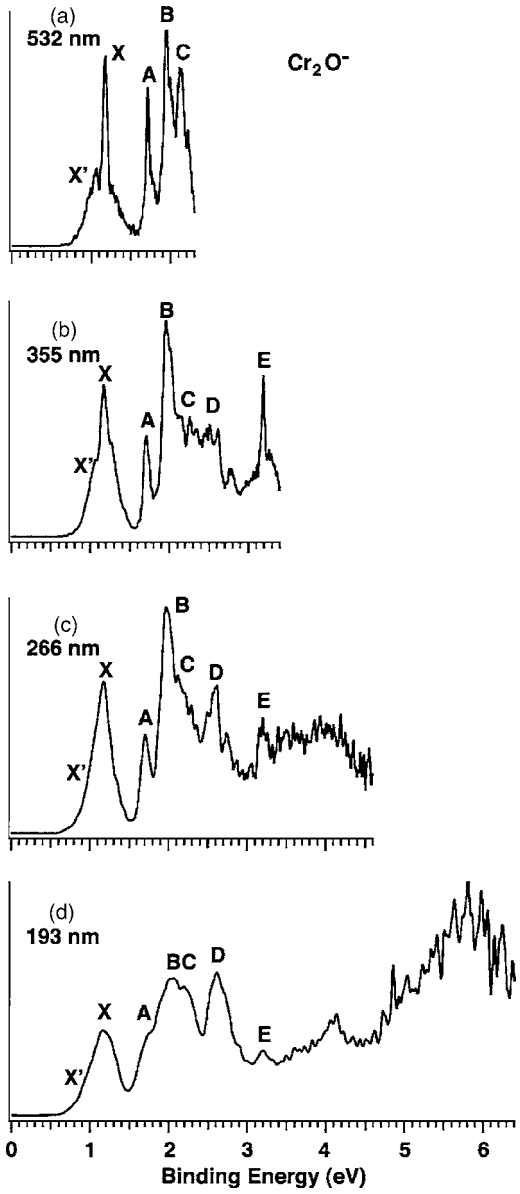

FIG. 1. Photoelectron spectra of Cr_2O^- at (a) 532 nm (2.331 eV), (b) 355 nm (3.496 eV), (c) 266 nm (4.661 eV), and (d) 193 nm (6.424 eV).

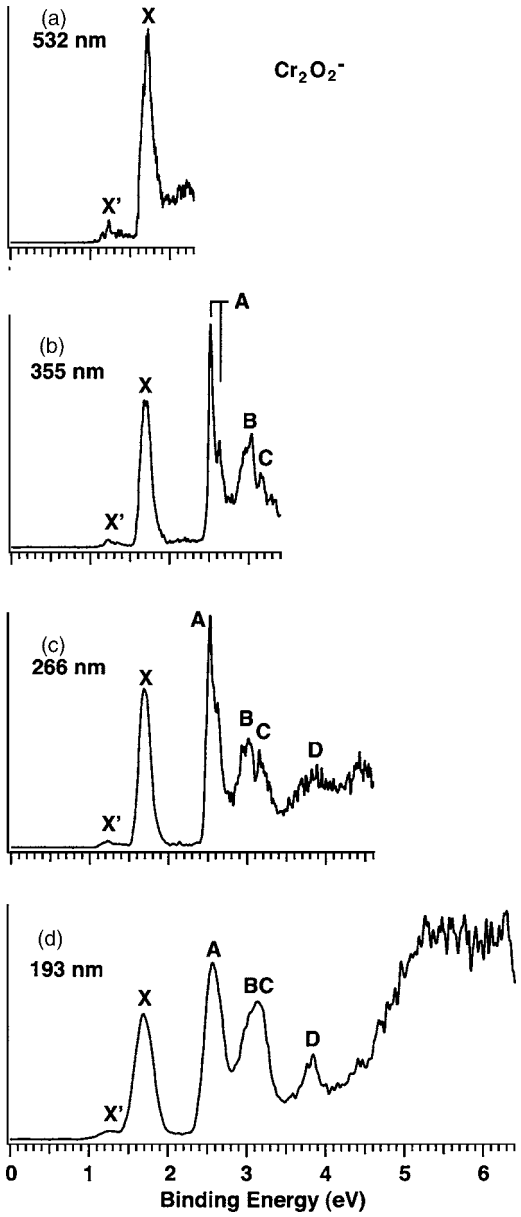

FIG. 2. Photoelectron spectra of $Cr_2O_2^-$ at (a) 532, (b) 355, (c) 266, and (d) 193 nm. The vertical bars represent the resolved vibrational structures.

very weakly populated low-lying isomer. At 355 nm [Fig. 2(b)], three more bands *A*, *B*, and *C* were revealed at VDEs of 2.52, 2.99, and 3.16 eV, respectively, following a significant energy gap of ~0.8 eV after the *X* band. Band *A* was vibrationally resolved with a short vibrational progression and a spacing of 890 cm^{-1}. At 266 nm [Fig. 2(c)], a rather broad band (*D*) was observed at ~3.8 eV, which became better defined at 193 nm. However, beyond 4 eV the 193 nm spectrum became continuous without any resolved features.

C. $Cr_2O_3^-$

Figure 3 shows the PES spectra of $Cr_2O_3^-$ at four photon energies. The 532 nm spectrum revealed the ground state transition *X* with rich fine features. As shown in the inset of Fig. 3(a), a total of nine peaks were resolved (*a*: 1.68 eV, *b*: 1.71 eV, *c*: 1.75 eV, *d*: 1.79 eV, *e*: 1.83 eV, *f*: 1.87 eV, *g*: 1.91 eV, *h*: 1.94 eV, and *i*: 1.98 eV), which appeared to be due to two vibrational progressions, a high frequency mode with a spacing of 620 cm^{-1} and a low frequency mode with a frequency ~280 cm^{-1}. The ADE of band *X* was defined by the fine feature *a* at 1.68 eV, whereas the VDE of band *X* was defined by the feature *e* at 1.83 eV. At 355 nm, a broad band *A* was observed with a VDE of 2.36 eV [Fig. 3(b)]. Two relatively sharp bands *B* and *C* were also observed at higher binding energies with VDEs of 3.01 and 3.14 eV, respectively. The 266 and 193 nm spectra revealed congested PES features at higher binding energies. Two broad features *D* and *E* could be tentatively identified.

We observed that under hot source conditions the relative intensity of band *X* appeared to increase. Figure 4 shows a 193 nm spectrum measured by using 0.5% O_2 seeded He carrier gas, which produced relatively hot clusters. The intensity increase of band *X* under the hot source conditions suggested that it contained contributions from a low-lying isomer.

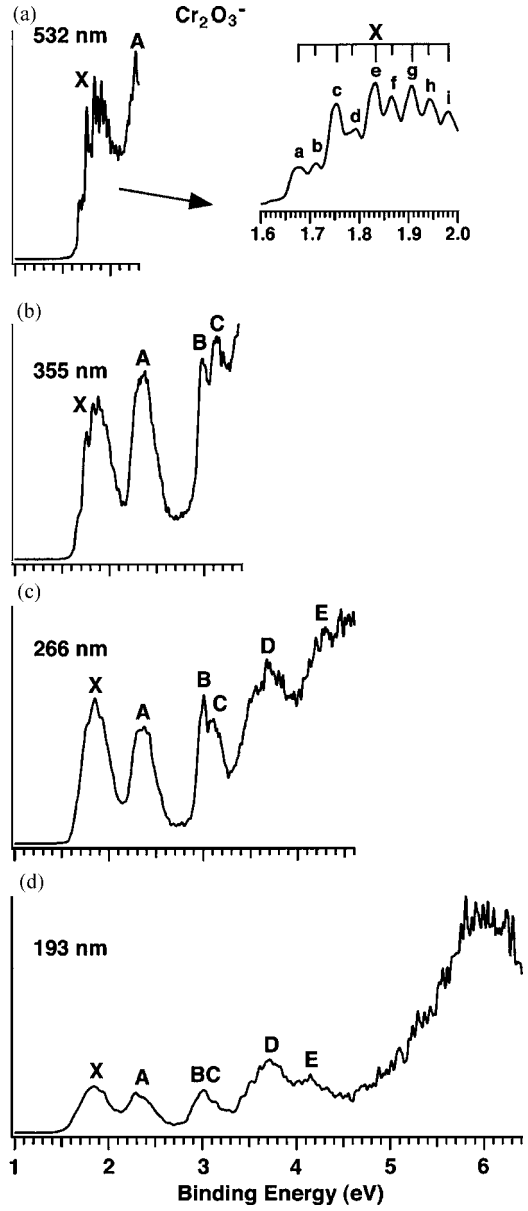

FIG. 3. Photoelectron spectra of $Cr_2O_3^-$ at (a) 532, (b) 355, (c) 266, and (d) 193 nm. The inset in (a) shows the fine features within band *X*.

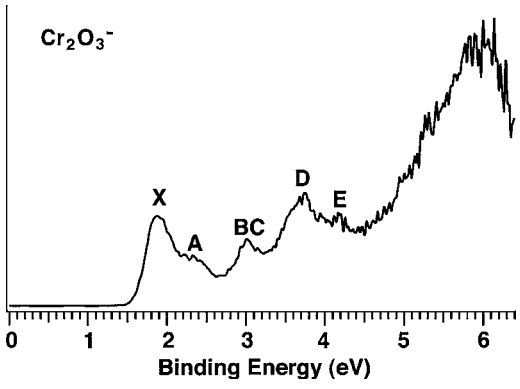

FIG. 4. 193 nm photoelectron spectra of $Cr_2O_3^-$ under hot source conditions by using 0.5% O_2 seeded He carrier gas. Note the relative intensity of band *X* increased markedly relative to Fig. 3(d), indicating contributions from a low-lying isomer.

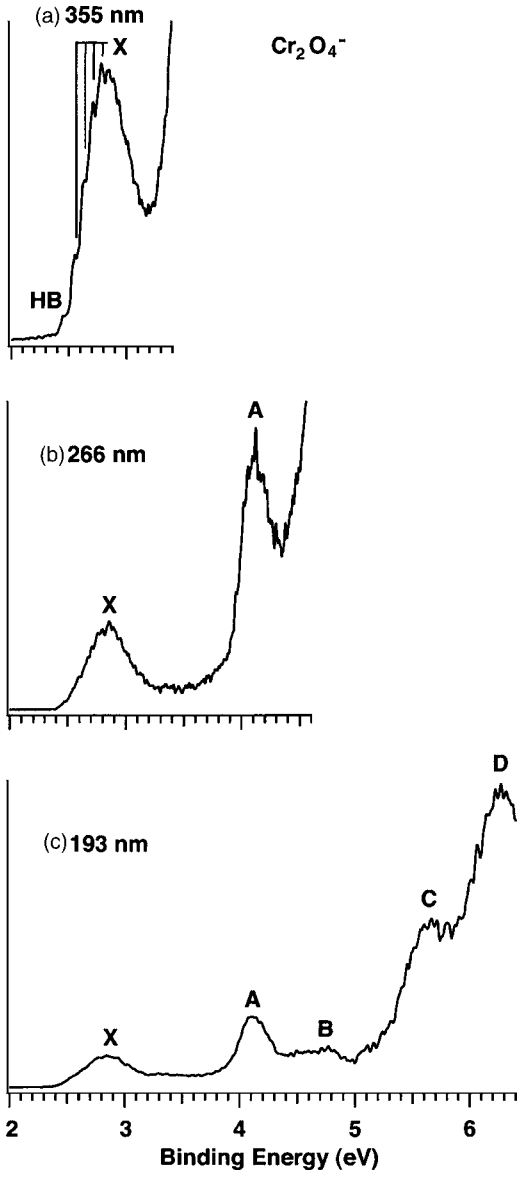

FIG. 5. Photoelectron spectra of $Cr_2O_4^-$ at (a) 355, (b) 266, and (c) 193 nm. The vertical bars represent the resolved vibrational structures. "HB" stands for a hot band transition.

D. $Cr_2O_4^-$

Due to the increase of electron binding energies, we could only measure the spectra of $Cr_2O_4^-$ at 355, 266, and 193 nm, as shown in Fig. 5. The 355 nm spectrum [Fig. 5(a)] revealed a broad band for the ground state transition (*X*) with discernible fine features. The lower binding energy part of the band appeared to be better resolved than the higher binding energy part, and a vibrational spacing of 630 cm^{-1} could be identified. The ADE and VDE of band *X* were evaluated to be 2.55 and 2.84 eV, respectively. The lowest binding energy peak, labeled "HB," was assigned as a hot band transition because of its larger spacing from the 0-0 transition. The 266 nm spectrum [Fig. 5(b)] resolved a second band *A* at a VDE of 4.12 eV, following a large energy gap of ~1.3 eV from band *X*. At 193 nm, three more broad bands were observed. Band *B* at 4.70 eV was relatively weak, whereas bands *C* and *D* were both very intense.

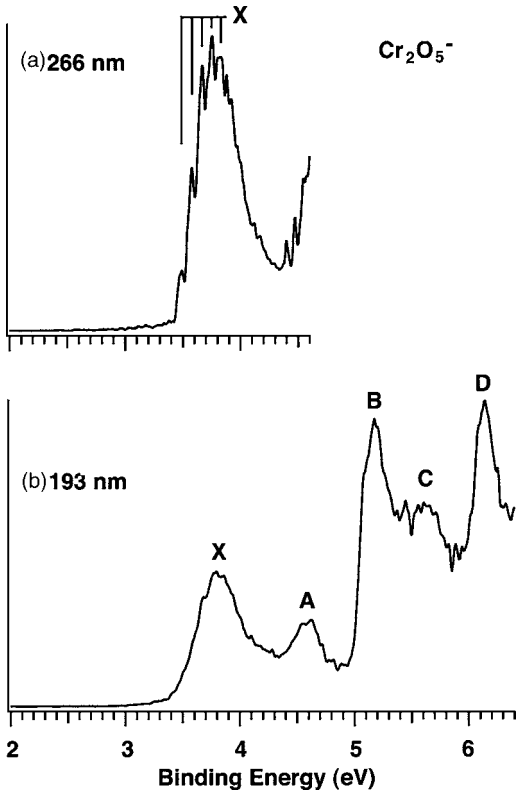

FIG. 6. Photoelectron spectra of $Cr_2O_5^-$ at (a) 266 and (b) 193 nm. The vertical bars represent the resolved vibrational structures.

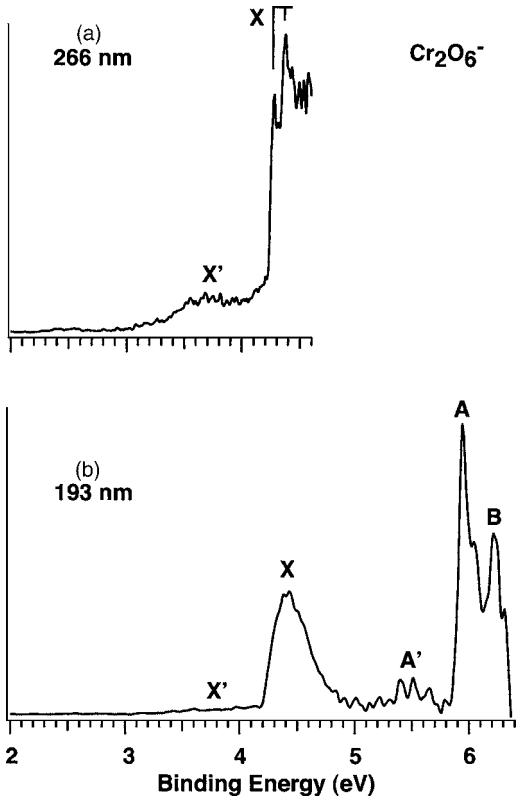

FIG. 7. Photoelectron spectra of $Cr_2O_6^-$ at (a) 266 and (b) 193 nm. The vertical bars represent the resolved vibrational structures.

E. $Cr_2O_5^-$

Only 266 and 193 nm photons were able to access detachment transitions for $Cr_2O_5^-$, as shown in Fig. 6. The 266 nm spectrum revealed the ground state transition (X) with a partially resolved vibrational progression and a spacing of 710 cm^{-1}, similar in shape to the ground state transition in $Cr_2O_4^-$ [Fig. 5(a)]. The ADE and VDE for the ground state transition were measured to be 3.49 and 3.82 eV, respectively. At 193 nm, four more bands, A, B, C, and D, were revealed at 4.58, 5.17, 5.60, and 6.13 eV, respectively.

F. $Cr_2O_6^-$

Similar to $Cr_2O_5^-$, only 266 and 193 nm photons were able to detach electrons from $Cr_2O_6^-$, as shown in Fig. 7. The 266 nm spectrum revealed the ground state transition X, which showed a partially resolved vibrational progression with a spacing of 780 cm^{-1}. The 0-0 transition defined an ADE of 4.28 eV. A weak and broad feature X' was observed at lower binding energies. The 193 nm spectrum [Fig. 7(b)] resolved two intense and sharp bands at higher binding energies, A (VDE: 5.98 eV) and B (VDE: 6.28 eV), following a large gap (~1.7 eV) from the X band. However, some weak signals (A') were also observed in the gap region. Under hot source conditions, we found that bands X' and A' were significantly enhanced (Fig. 8), suggesting that they were due to a low-lying isomer.

G. $Cr_2O_7^-$

We recently reported the PES spectra of $Cr_2O_7^-$ along with other $M_2O_7^{2-}$ and $M_2O_7^-$ (M=Cr, Mo, W) species at 193 and 157 nm, as well as DFT calculations on the W species.[35] For completeness, the 193 nm spectrum of $Cr_2O_7^-$ is again presented in Fig. 9, where it is compared to the other $Cr_2O_n^-$ species. The $Cr_2O_7^-$ spectrum revealed a ground state transition and a partial band for the first excited state at very high electron binding energies. The ground state transition was well-defined with a VDE of 5.90 eV and an ADE of 5.57 eV.[35]

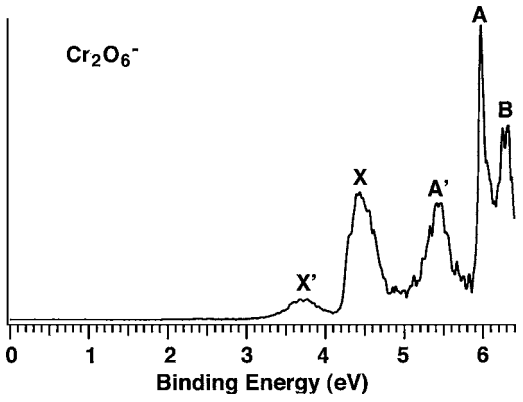

FIG. 8. 193 nm photoelectron spectra of $Cr_2O_6^-$ under hot source conditions by using 0.5% O_2 seeded He carrier gas. Note the relative intensities of bands X' and A' were significantly enhanced relative to Fig. 7(b), indicating the coexistence of two isomers in the $Cr_2O_6^-$ cluster beam.

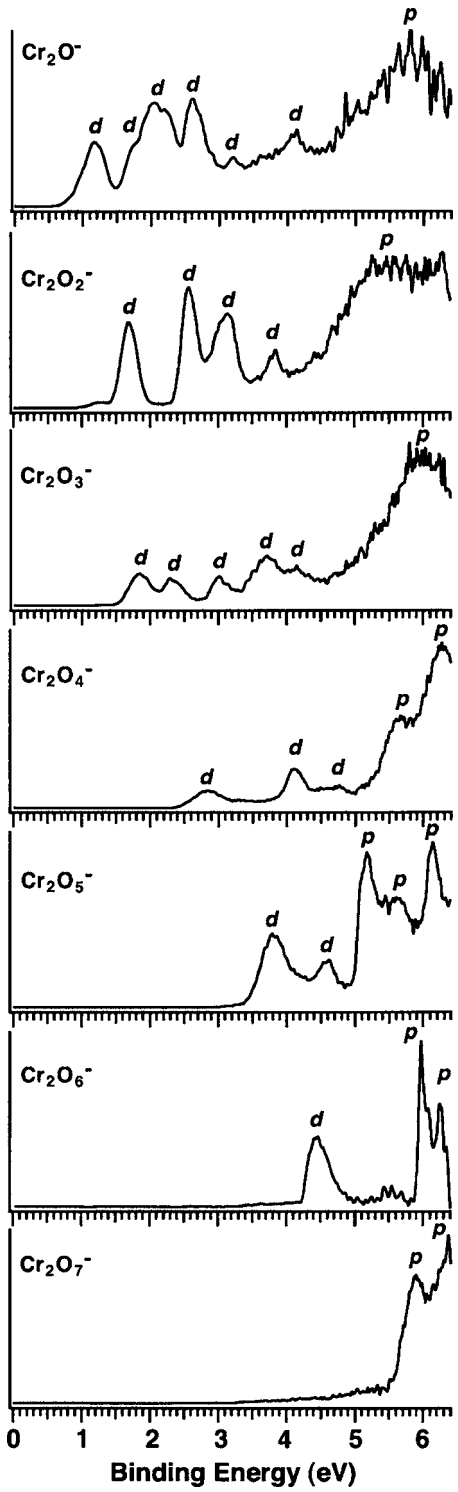

FIG. 9. Comparison of the 193 nm photoelectron spectra of $Cr_2O_n^-$ (n=1–7). d denotes photodetachment transitions from Cr 3d-derived orbitals and p denotes those from O 2p-derived orbitals.

IV. DISCUSSION

A. Cr_2O^- and $Cr_2O_2^-$: Ferromagnetic clusters

Cr_2O^- and $Cr_2O_2^-$ and their neutrals were investigated both experimentally[9–11] and theoretically[5–10] in several previous studies. Kondow and co-workers[9,10] recently reported a combined PES and DFT study on $Cr_2O_n^-$ (n=1–3), in which relatively low resolution 355 nm spectra were presented and compared with their DFT calculations. The ground state of Cr_2O^- was predicted to be a high spin state (S=9/2) (ferromagnetic) with C_{2v} symmetry and a long Cr–Cr distance of 2.85 Å. The low spin isomer (S=1/2) (antiferromagnetic) was found to be 1.6 eV higher in energy with a much shorter Cr–Cr distance of 1.83 Å. They made semiquantitative spectral assignments according to their DFT calculations and identified three bands (X, A, and B), which were consistent with the current 266 nm data. However, in the current study the lowest energy band was resolved into a sharp peak X and a broad band X' [Fig. 1(a)], which were thought to be one broad band by Kondow and co-workers,[9,10] as that shown in the 266 nm spectrum [Fig. 1(c)]. Our observation calls for a new spectral assignment, as shown in Table II.

TABLE II. Comparison of the observed detachment transitions with previous DFT calculations from Ref. 10. All energies are in eV.

	Current VDE	Theoretical VDE (final state)[a]
$Cr_2O^-(^{10}B_2)$	1.1 (X')	1.08 ($^{11}B_2$)
	1.17 (X)	1.65 ($^9A_2$)
	1.71 (A)	1.68 ($^9A_1$)
	1.95 (B)	2.18 ($^9B_2$)
	2.1–2.9 (C and D)	2.48 ($^9A_1$), 2.53 ($^9B_1$), 2.58 ($^9A_1$), 2.75 ($^9B_1$), 2.76 ($^9B_1$), 2.86 ($^9A_2$), 2.96 ($^9B_2$)
$Cr_2O_2^-(^{10}A_{1g})$	1.69 (X)	1.69 ($^9A_{1g}$)[b]
	2.52 (A)	2.41 ($^9B_{3g}$)[b]
	2.99 (B)	3.03 ($^9B_{3u}$),[b] 3.06 ($^9B_{1u}$)[b]
	3.16 (C)	3.28 ($^9A_{1g}$)[b]
	3.81 (D)	3.66 ($^9B_{2g}$),[b] 3.67 ($^9B_{3u}$)[b]
$Cr_2O_3^-(^8A')$	1.85 (X)	2.08 ($^7A'$)
	2.36 (A)	2.32 ($^7A''$)
	3.01 (B)	2.93 ($^7A'$)

[a]From Ref. 10.
[b]All calculated VDEs for $Cr_2O_2^-$ are shifted to higher binding energies by 0.56 eV relative to that computed from DFT in Ref. 10. For example, the first computed VDE from Ref. 10 was 1.13 eV ($^9A_{1g}$).

Kondow and co-workers assigned the ground state transition with a calculated VDE of 1.08 eV ($^{11}B_2$, Table II) to the broad X band in their spectrum and assigned the transitions at VDEs 1.65 eV ($^9A_2$) and 1.68 eV ($^9A_1$) to the A band, which was less well resolved in the previous study. Clearly, these assignments need revisions in light of the current data, because (1) the band A is in fact very sharp and is unreasonable to be assigned to two electronic transitions (Fig. 1) and (2) two electronic states are now resolved in the low binding energy band (X' and X). We propose to reassign the spectral transitions, as given in Table II. In the new assignment, the ground state transition ($^{11}B_2$) is assigned to the broad band X', the $^9A_2$ transition to the X band, and the $^9A_1$ transition to the A band. Kondow and co-workers' DFT calculations showed that there is a large geometry change in the ∠Cr–O–Cr angle between the ground states of Cr_2O^- and Cr_2O, consistent with the broad X' band. They also found that there is less geometry change for the transitions to the $^9A_2$ and $^9A_1$ excited states, consistent with the sharper peaks observed for bands X and A. The reassignment suggests that

there is a large error for the computed VDE for the $^9A_2$ state. However, the calculated VDEs for all other transitions seem to be in quite good agreement with the experiment, as shown in Table II. There are numerous unresolved features in the spectral region of bands *C* and *D* (Fig. 1), which are consistent with the DFT results that showed at least seven transitions in the same energy range. Therefore, we conclude that the overall agreement between the current PES data and the previous DFT calculations is reasonable, confirming the high spin ground states for both Cr_2O^- and Cr_2O.

For $Cr_2O_2^-$, Tono *et al.*[10] observed the first four bands including the low binding energy weak feature (X',X,A,B). However, they assigned the very weak band X' as the ground state transition, which differs from our assignment. From our experiences, such a weak signal was most likely due to a low-lying isomer, even though we were not able to alter its relative intensity because of the weak mass signals from our cluster source, allowing only a narrow parameter space to produce sufficient $Cr_2O_2^-$ clusters for the PES experiment. The DFT calculations of Tono *et al.*[10] predicted again a high spin ground state ($S=9/2$) for $Cr_2O_2^-$ with rhombus D_{2h} symmetry and a large Cr–Cr distance of 2.64 Å. A low spin ($S=1/2$) isomer with similar D_{2h} symmetry but a shorter Cr–Cr distance of 2.01 Å was found to be 1.4 eV higher in energy. They also made spectral assignments based on the DFT calculations. They predicted a relatively small VDE (1.13 eV) for the ground state transition, which might be the motivation for them to assign the weak signal X' as the ground state transition. But the overall agreement between their calculated VDEs for the high spin $Cr_2O_2^-$ and their experimental data was not very satisfactory. However, we noticed that their calculated spectral pattern agrees well with our spectra, which were better resolved and contained more spectral transitions. In particular, we found that if we added a constant of 0.56 eV to their calculated VDEs, the corrected VDEs are in excellent agreement with our PES data, as shown in Table II. We tentatively take this agreement as evidence for the high spin ground state for $Cr_2O_2^-$. Clearly, more accurate calculations are warranted in light of the current data.

B. $Cr_2O_3^-$: Ferromagnetic versus antiferromagnetic isomers

The 355 nm spectrum of $Cr_2O_3^-$ by Tono *et al.*[10] resolved only bands *X* and *A*. However, the relative ratio of their bands *X* and *A* is very different from our data. In our 355 nm spectrum [Fig. 3(b)], bands *X* and *A* are both very intense with band *A* being slightly stronger. But in their 355 nm spectrum, band *X* was much stronger, at least twice as intense as band *A*. Our temperature-dependent study (Fig. 4) suggested that the 355 nm spectrum by Kondow and coworkers might be taken at relatively high temperature conditions and contained large contributions from a low-lying isomer.

DFT calculations by Tono *et al.*[10] predicted that $Cr_2O_3^-$ possesses C_s symmetry and a puckered four-membered ring structure with an extra oxygen atom terminally bonded to one Cr atom. They found that a high spin state ($S=7/2$) and a low spin state ($S=1/2$) were nearly degenerate with the low spin state only 0.04 eV higher in energy. The predicted first VDEs for both isomers were similar. Our current PES data matches the predicted VDE pattern of the high spin species ($^8A'$) rather well (see Table II), and disagrees with that of the low spin species ($S=1/2$). We therefore conclude that the dominant species observed in our experiment was due to the high spin isomer with the low spin isomer contributing to the *X* band under high temperature conditions. The two vibrational modes observed in our PES spectrum for the ground state transition [Fig. 3(a)] were probably due to Cr–O stretching for the high frequency mode (620 cm^{-1}) and a bending motion for the low frequency mode (280 cm^{-1}).

C. $Cr_2O_4^-$, $Cr_2O_5^-$, and $Cr_2O_6^-$

There are no previous experiments on the high oxygen content oxide clusters, but there have been several theoretical calculations about the Cr_2O_n neutral clusters ($n=4-6$).[5,6,8] Cr_2O_4 was suggested to possess a puckered structure with a four-membered ring and two terminal O atoms each bonded to a Cr atom. This structure is similar to those for the isoelectronic W_2O_4 and Mo_2O_4 studied previously.[34,39] The ground state of Cr_2O_4 was predicted to be a triplet state, also similar to W_2O_4 and Mo_2O_4. Without detailed calculations on the $Cr_2O_4^-$ anion, it is difficult to make detailed assignments of the PES features. The observed vibrational progression (630 cm^{-1}) in the ground state band [Fig. 5(a)] is most likely due to a Cr–O stretching mode. The congested nature of the *X* band suggested that there might also be low frequency bending modes excited during the detachment transition.

The structure of Cr_2O_5 was predicted to be similar to that of Cr_2O_4 with the extra O atom bonded to one Cr atom.[5,6] This structure is similar to that found for W_2O_5.[34] The ground state of Cr_2O_5 was predicted to be a singlet, also similar to W_2O_5. The observed vibrational progression (710 cm^{-1}) for the ground state transition [Fig. 6(a)] is likely due to a Cr–O stretching mode.

Cr_2O_6 is a stoichiometric cluster and its structure was predicted to be D_{2h} with a four-membered ring and two terminal O atoms on each Cr,[5,6] which is identical to W_2O_6.[34] The observed PES spectrum for $Cr_2O_6^-$ showed a large highest occupied molecular orbital (HOMO)-lowest unoccupied molecular orbital (LUMO) gap (~1.7 eV), consistent with a stable closed shell Cr_2O_6 neutral cluster. The LUMO of Cr_2O_6, where the extra electron resides in $Cr_2O_6^-$, should be a *d*-type orbital delocalized on the two Cr atoms, similar to that in $W_2O_6^-$.[34] Thus the observed vibrational progression in the ground state transition [Fig. 7(a)] should be due to a Cr–O stretching mode. The vibrational progression observed in the ground state transition in $Cr_2O_6^-$ is also similar to that in $W_2O_6^-$, but the vibrational frequency in Cr_2O_6 (710 cm^{-1}) is much smaller than that in W_2O_6 (920 cm^{-1}), consistent with the fact that the W–O bond is stronger than the Cr–O bond.[33]

It was interesting that a low-lying isomer was observed for $Cr_2O_6^-$ (Fig. 8). Even under the relatively cold source conditions, the low-lying isomer could not be completely

eliminated, suggesting that it is probably very close in energy to the D_{2h} ground state. A possible candidate for this isomer is a peroxy-type structure, i.e., a $Cr_2O_4^-$ structure with an O_2 unit bonded to one Cr atom. Such a structure would be similar to $Cr_2O_5^-$, in that an O atom is replaced by an O_2 peroxy unit. Indeed, the binding energy of this isomer is lower and is similar to that of $Cr_2O_5^-$. It was surprising to observe such an isomer for the stoichiometric $Cr_2O_6^-$ cluster. We have observed peroxy-type oxide clusters previously, but usually in O-rich clusters, such as CrO_5 or W_2O_7.[31,35]

D. Overall spectral evolution of $Cr_2O_n^-$ (n=1–7) and sequential oxidation

As shown in our previous work on $Al_3O_n^-$, $V_2O_n^-$, and $W_2O_n^-$,[29,32,34] metal-based photodetachment features can be easily distinguished from O 2p-based features in O-deficient metal oxide clusters. Specifically, O 2p-based features typically appear at binding energies beyond ~5 eV, whereas features at lower binding energies are normally metal based. This is clearly also the case for the $Cr_2O_n^-$ series as can be seen in Fig. 9, where features at lower binding energies (<5 eV) are labeled as d (Cr 3d) and those above 5 eV are labeled as p (O 2p). The general observation is consistent with the detailed density of states (DOS) analyses for Cr_2O^-, $Cr_2O_2^-$, and $Cr_2O_3^-$ from previous DFT calculations by Kondow and co-workers.[9,10] These authors showed that the DOS within ~3 eV below the Fermi level is primarily contributed from the majority Cr 3d electrons, whereas the DOS due to the O 2p electrons are mainly located at 4–6 eV below the Fermi level. As n increases in $Cr_2O_n^-$, the d bands at lower binding energies diminish and the electron binding energies increase as a result of electron transfer from Cr to O. At n=6, the bulk stoichiometry is reached and all the electrons are transferred to O, resulting in a stable closed-shell Cr_2O_6 cluster, as shown by the large HOMO-LUMO gap observed in the 193 nm spectrum of $Cr_2O_6^-$. $Cr_2O_7^-$ is an O-rich cluster and there are no longer d-type PES features at lower binding energies. All the observed bands for $Cr_2O_7^-$ are O 2p based with extremely high binding energies beyond 5.5 eV (Fig. 9). The electron affinity of Cr_2O_7 was measured to be 5.57±0.05 eV, which is among the highest ever reported for metal oxide clusters.[31–33,36,37,47] All these observations showed the trend of sequential oxidation in the $Cr_2O_n^-$ series. The simple picture of sequential oxidation is a useful concept in elucidating the electronic structure of metal oxide clusters and understanding their chemical properties.[25,26,29,32,34]

E. Comparison between the electronic structures of $Cr_2O_n^-$ and $W_2O_n^-$

Recently, we have reported a detailed study combining PES and DFT calculations on $W_2O_n^-$ clusters,[34] which are isoelectronic with $Cr_2O_n^-$. Thus, it would be interesting to compare the two systems. Jarrold and co-workers have studied several clusters of $Mo_2O_n^-$,[39,40] which are in general similar to the $W_2O_n^-$ systems. There are two major differences between the 3d and 5d metals, which are relevant to properties of their oxides. First, the 3d orbitals are more compact and form weaker metal-metal bonds relative to the 5d orbitals, resulting in interesting magnetic couplings in the 3d metals, whereas the 5d metals are nonmagnetic due to strong d-d bonding. The second difference between W and Cr is that W forms much stronger bonds with O than Cr does.[33]

Major differences between the Cr_2O_n and W_2O_n clusters occur for the very O-deficient systems from n=1–3 both structurally and electronically. Oxidation of the Cr_2 dimer by one to three O atoms transforms an antiferromagnetic Cr_2 into ferromagnetic Cr_2O_n oxide clusters.[5–10] Although the ground state of W_2O is a triplet state, both the ground state of W_2O_2 and W_2O_3 are singlets and nonmagnetic. The structures of the two systems are also very different. Whereas in Cr_2O_n the first two O atoms bond to both Cr atoms in a bridging manner, in W_2O_n the first two O atoms each bond only to one W atom because of the strong W–O bond strength.[34] This leaves strong W–W bonding in the O-deficient W_2O_n clusters, resulting in nonmagnetic or very weak magnetic systems. For n=4 and higher, the Cr_2O_n and W_2O_n systems become similar as the magnetic coupling in the Cr systems becomes weakened due to the loss of 3d electrons to oxygen. One interesting observation is the existence of a low-lying isomer in $Cr_2O_6^-$. No low-lying isomer was observed for $W_2O_6^-$ due to the overwhelming stability of the D_{2h} structure, which is also reflected in the much larger HOMO-LUMO gap in W_2O_6, 2.8 eV vs 1.7 eV in Cr_2O_6.

V. CONCLUSIONS

We report a systematic photoelectron spectroscopic study on a series of dichromium oxide clusters, $Cr_2O_n^-$ (n=1–7). Well-resolved PES spectra are obtained for each species at different photon energies. The results are compared with previous studies[9,10] for n=1–3 and reassignments of major spectral features are made as a result of the better resolved spectra. The overall PES evolution exhibits a behavior of sequential oxidation with oxygen content, where low binding energy Cr 3d-based spectral features diminish in numbers and the spectra shift towards higher binding energies as a result of charge transfer from Cr to O. Clear evidence is also obtained for the existence of low-lying isomers for $Cr_2O_2^-$, $Cr_2O_3^-$, and $Cr_2O_6^-$. Differences between the $Cr_2O_n^-$ and $W_2O_n^-$ systems are discussed.

ACKNOWLEDGMENTS

This work was supported by the Chemical Sciences, Geosciences and Biosciences Division, Office of Basic Energy Sciences, U.S. Department of Energy under Grant No. DE-FG02-03ER15481 (catalysis center program) and was performed at the W. R. Wiley Environmental Molecular Sciences Laboratory, a national scientific user facility sponsored by DOE's Office of Biological and Environmental Research and located at Pacific Northwest National Laboratory, operated for DOE by Battelle.

[1] N. N. Greenwood and A. Earnshaw, *Chemistry of the Elements*, 2nd ed. (Butterworth-Heinemann, Oxford, 1998).
[2] For a review, see B. M. Weckhuysen, I. E. Wachs, and R. A. Schoonheydt, Chem. Rev. (Washington, D.C.) **96**, 3327 (1996).
[3] R. A. de Groot, F. M. Mueller, P. G. van Engen, and K. H. J. Buschow, Phys. Rev. Lett. **50**, 2024 (1983).

[4] M. A. Korotin, V. I. Anisimov, D. I. Khomskii, and G. A. Sawatzky, Phys. Rev. Lett. **80**, 4305 (1998).
[5] B. V. Reddy and S. N. Khanna, Phys. Rev. Lett. **83**, 3170 (1999).
[6] B. V. Reddy, S. N. Khanna, and C. Ashman, Phys. Rev. B **61**, 5797 (2000).
[7] S. Veliah, K. H. Xiang, R. Pandey, J. M. Recio, and J. M. Newsam, J. Phys. Chem. B **102**, 1126 (1998).
[8] K. H. Xiang, R. Pandey, J. M. Recio, E. Francisco, and J. M. Newsam, J. Phys. Chem. A **104**, 990 (2000).
[9] K. Tono, A. Terasaki, T. Ohta, and T. Kondow, Phys. Rev. Lett. **90**, 133402 (2003).
[10] K. Tono, A. Terasaki, T. Ohta, and T. Kondow, J. Chem. Phys. **119**, 11221 (2003).
[11] G. V. Chertihin, W. D. Bare, and L. Andrews, J. Chem. Phys. **107**, 2798 (1997).
[12] A. Hachimi, E. Poitevin, G. Krier, J. F. Miller, and M. F. Ruiz-Lopez, Int. J. Mass Spectrom. Ion Process. **144**, 23 (1995).
[13] M. J. Van Stipdonk, D. R. Justes, and E. A. Schweikert, Int. J. Mass. Spectrom. **203**, 59 (2000).
[14] F. Aubriet, B. Maunit, and J. F. Muller, Int. J. Mass. Spectrom. **209**, 5 (2001).
[15] A. K. Gianotto, B. D. M. Hodges, P. B. de Harrington, A. D. Appelhans, J. E. Olson, and G. S. Groenewold, J. Am. Soc. Mass Spectrom. **14**, 1067 (2003).
[16] D. E. Bergeron, A. W. Castleman, Jr., N. O. Jones, and S. N. Khanna, Nano Lett. **4**, 261 (2004).
[17] D. L. Michalopoulos, M. E. Geusic, S. G. Hansen, D. E. Powers, and R. E. Smalley, J. Phys. Chem. **86**, 3914 (1982).
[18] V. E. Bondybey and J. H. English, Chem. Phys. Lett. **94**, 443 (1983).
[19] S. J. Riley, E. K. Parks, L. G. Pobo, and S. Wexler, J. Chem. Phys. **79**, 2577 (1983).
[20] S. M. Casey and D. G. Leopold, J. Phys. Chem. **97**, 816 (1993).
[21] M. M. Goodgame and W. A. Goddard III, Phys. Rev. Lett. **54**, 661 (1985).
[22] B. Delley, A. J. Freeman, and D. E. Ellis, Phys. Rev. Lett. **50**, 488 (1983).
[23] H. S. Cheng and L. S. Wang, Phys. Rev. Lett. **77**, 51 (1996).
[24] N. Desmarais, F. A. Reuse, and S. N. Khanna, J. Chem. Phys. **112**, 5576 (2000).
[25] H. Wu, S. R. Desai, and L. S. Wang, J. Am. Chem. Soc. **118**, 5296 (1996).
[26] L. S. Wang, H. Wu, and S. R. Desai, Phys. Rev. Lett. **76**, 4853 (1996).
[27] L. S. Wang, H. Wu, S. R. Desai, and L. Lou, Phys. Rev. B **53**, 8028 (1996).
[28] L. S. Wang, J. B. Nicholas, M. Dupuis, H. Wu, and S. D. Colson, Phys. Rev. Lett. **78**, 4450 (1997).
[29] H. Wu, X. Li, X. B. Wang, C. F. Ding, and L. S. Wang, J. Chem. Phys. **109**, 449 (1998).
[30] L. S. Wang, in *Photoionization and Photodetachment*, Advanced Series in Physical Chemistry Vol. 10, edited by C. Y. Ng (World Scientific, Singapore, 2000), pp. 854–957.
[31] G. L. Gustev, P. Jena, H. J. Zhai, and L. S. Wang, J. Chem. Phys. **115**, 7935 (2001).
[32] H. J. Zhai and L. S. Wang, J. Chem. Phys. **117**, 7882 (2002).
[33] H. J. Zhai, B. Kiran, L. F. Cui, X. Li, D. A. Dixon, and L. S. Wang, J. Am. Chem. Soc. **126**, 16134 (2004).
[34] H. J. Zhai, X. Huang, L. F. Cui, X. Li, J. Li, and L. S. Wang, J. Phys. Chem. A **109**, 6019 (2005).
[35] H. J. Zhai, X. Huang, T. Waters, X. B. Wang, R. A. J. O'Hair, A. G. Wedd, and L. S. Wang, J. Phys. Chem. A **109**, 10512 (2005).
[36] X. Huang, H. J. Zhai, B. Kiran, and L. S. Wang, Angew. Chem., Int. Ed. **44**, 7251 (2005).
[37] X. Huang, H. J. Zhai, J. Li, and L. S. Wang, J. Phys. Chem. A **110**, 85 (2006).
[38] X. Huang, H. J. Zhai, T. Waters, J. Li, and L. S. Wang, Angew. Chem., Int. Ed. **45**, 657 (2006).
[39] B. L. Yoder, J. T. Maze, K. Raghavachari, and C. C. Jarrold, J. Chem. Phys. **122**, 094313 (2005).
[40] R. B. Wyrwas, B. L. Yoder, J. T. Maze, and C. C. Jarrold, J. Phys. Chem. A **110**, 2157 (2006).
[41] L. S. Wang, H. S. Cheng, and J. Fan, J. Chem. Phys. **102**, 9480 (1995).
[42] L. S. Wang and H. Wu, in *Cluster Materials*, Advances in Metal and Semiconductor Clusters Vol. 4, edited by M. A. Duncan (JAI, Greenwich, 1998), pp. 299–343.
[43] L. S. Wang and X. Li, in *Clusters and Nanostructure Interfaces*, edited by P. Jena, S. N. Khanna, and B. K. Rao (World Scientific, New Jersey, 2000), pp. 293–300.
[44] J. Akola, M. Manninen, H. Hakkinen, U. Landman, X. Li, and L. S. Wang, Phys. Rev. B **60**, 11297 (1999).
[45] L. S. Wang, X. Li, and H. F. Zhang, Chem. Phys. **262**, 53 (2000).
[46] H. J. Zhai, L. S. Wang, A. N. Alexandrova, and A. I. Boldyrev, J. Chem. Phys. **117**, 7917 (2002).
[47] J. C. Rienstra-Kiracofe, G. S. Tschumper, H. F. Schaefer III, S. Nandi, and G. B. Ellision, Chem. Rev. (Washington, D.C.) **102**, 231 (2002).